Geophys. J. Int. (1998) **135,** 313–328

Current plate motions across the Red Sea

Dezhi Chu and Richard G. Gordon

Department of Geology & Geophysics, Rice University, Houston, TX 77005, *USA. E-mail: rgg@geophysics.rice.edu*

Accepted 1998 May 12. Received 1998 April 16; in original form 1997 June 20

SUMMARY

A new objective method is used to estimate precisely 64 rates of seafloor spreading since chron 2A (3.2 Ma) from all the Red Sea magnetic profiles available from 15.9° to 26°N. The fastest spreading rate, $\approx$16 mm yr^{-1}, occurs near 18°N, whereas the slowest rate, 10 mm yr^{-1}, occurs at 25.5°N and is consistent with the rate predicted from Arabia–Nubia data to the south. The standard deviation of the spreading rates is 0.8 mm yr^{-1}, much smaller than the median standard deviation of 4 mm yr^{-1} previously assigned to spreading rates in the global plate-motion model NUVEL-1 (DeMets *et al.* 1990). The fit to the spreading rates, as well as the locations of earthquakes in and near the Red Sea, indicate that spreading south of approximately 17.7°N is less than the full rate of spreading between the Arabian and Nubian plates. The Red Sea spreading centre is instead usefully interpreted as the boundary between the Arabian Plate and a Danakil microplate that includes the subaerial Danakil block and a larger oceanic portion of lithosphere. Despite the absence of reliable azimuths of transform faults in the Red Sea, all components of the angular velocity of Arabia relative to Nubia are usefully constrained from just the 45 relevant spreading rates. The new compact 95 per cent confidence region of the angular velocity excludes prior estimates based on only four and two spreading rates by Chase (1978) and Jestin *et al.* (1994), respectively. 19 spreading rates in the southern Red Sea are used to estimate the angular velocity between the Danakil microplate and Arabia. An approach based on singular value decomposition shows that without slip vectors only two of the three components of the angular velocity of the Danakil microplate relative to Arabia or Nubia are usefully constrained, but that all three components are usefully constrained if one earthquake slip vector is included.

Key words: plate motion, Red Sea, seafloor spreading.

INTRODUCTION

Current plate motions across and near the Red Sea have proved di cult to estimate accurately. The Arabian Plate separates from the Nubian Plate across the Red Sea and separates from the Somalian Plate across the Sheba Ridge in the Gulf of Aden. The Nubian and Somalian plates in turn separate slowly across the East African Rift system. Motion between the Nubian and Somalian plates has not been estimated directly, but in the absence of long-baseline geodetic data must instead be inferred by subtracting the motion of Nubia relative to Arabia from that of Somalia relative to Arabia. Although the latter angular velocity is well determined, the former is much less accurately known. For example, DeMets *et al.* (1990), like Minster & Jordan (1978), found that it was too uncertain to be incorporated into a self-consistent global plate-motion model. For the most recently published angular velocity of Arabia relative to Nubia, only two spreading rates from the Red Sea were used in estimating the angular velocity of Arabia relative to Nubia (Jestin *et al.* 1994). Here we remedy the scarceness of useful spreading rates by analysing all available magnetic anomaly profiles from the Red Sea, from which we determine 64 useful spreading rates.

Three issues arise in investigating the current plate motions across the Red Sea. First, do azimuths of transform faults in the Red Sea usefully constrain the direction of relative plate motion, as assumed in some prior work (Bäcker *et al.* 1975; Le Pichon & Francheteau 1978; Chase 1978; Jestin *et al.* 1994)? We think not. Geophysical surveys show that any possible o sets of the Red Sea spreading centre are small, less than 5 km (Garfunkel *et al.* 1987; Izzeldin 1989). The strikes of many faults with o sets less than 35 km, especially along the Mid-Atlantic Ridge, di er significantly from the direction of relative plate motion (Searle & Laughton 1977), which is why DeMets *et al.* (1990) required that a transform fault o set a spreading centre by at least 35 km for its azimuth to be accepted into the data set used to construct global plate-motion model NUVEL-1. The incorporation of azimuths from these short faults in the Red Sea causes the uncertainty in relative plate motion to be underestimated, and might

introduce a bias in the direction of motion. Here we show that an accurate and useful angular velocity of Nubia relative to Arabia can be obtained from rates alone. There is thus no need to incorporate unreliable directional data.

Second, is the motion between the Nubian and Arabian plates localized as seafloor spreading everywhere along the Red Sea, or is additional motion accommodated across a wider zone? Seismicity along the axis of the Red Sea divides into two distinct branches near $\approx 17.5^{\circ}$N (Fig. 1). One branch continues SE along the axis of the Red Sea and a second branch continues SSW to where it eventually joins two lines of earthquakes, one that comprises the northernmost earthquakes of the East African Rift System and a second line that continues eastwards to the Gulf of Tadjurah, the narrow westward continuation of the Gulf of Aden (Fig. 1). The two branches of seismicity emanating from $\approx 17.5^{\circ}$N in the Red Sea and the line of seismicity west of the Gulf of Tadjurah together surround a relatively aseismic area that includes the subaerial Danakil block or crank-arm (Sichler 1980). Here we interpret this continental block and adjacent seafloor SW of the Red Sea spreading ridge as a microplate (Le Pichon & Francheteau 1978). We use our new set of spreading rates to determine whether motion of this Danakil microplate relative to the Nubian Plate is resolvable, to investigate where the plate-motion data indicate that Nubia ends and the microplate begins, and to estimate the motion of the microplate relative to the surrounding plates.

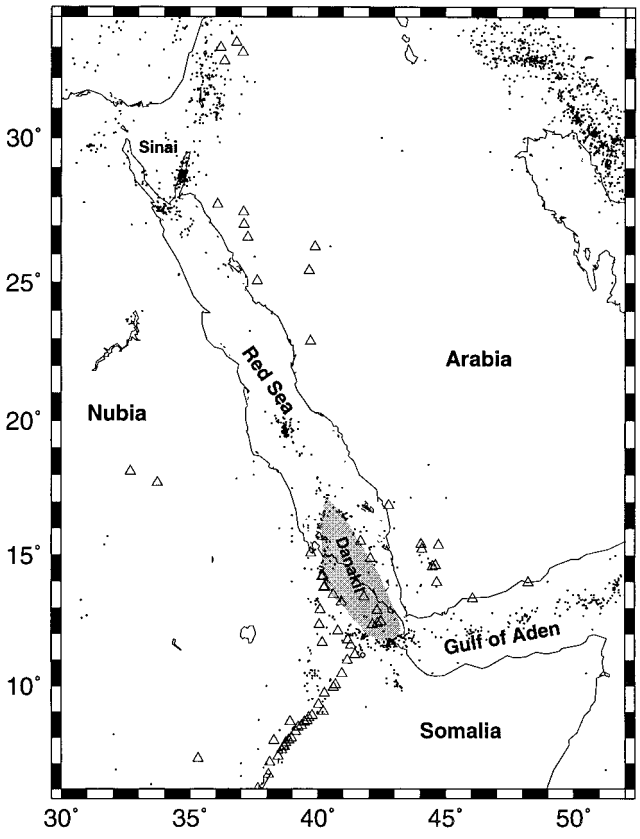

Figure 1. Location map of the study area. Small dots are epicentres of earthquakes from 1950 to 1993. Triangles show locations of volcanoes (Simkin *et al.* 1989). The open circles show the locations of the ridge crossings for spreading rates used in this paper. The shaded region shows the approximate extent of the Danakil microplate.

Third, should the Sinai block be included as part of the Nubian Plate? If included, then data along the Dead Sea fault could be used to improve estimates of motion between Nubia and Arabia. Unfortunately, the Sinai block is evidently separated from the Nubian Plate by a band of earthquakes (Fig. 1), including two instrumented earthquakes of magnitudes 6.2 M_s and 6.1 M_s (Huang & Solomon 1987) and a historical earthquake of about magnitude 6.6 (Ambraseys *et al.* 1994). Bosworth & Taviani (1996) estimated a 0.8–1.2 mm yr^{-1} rate of separation of Nubia from Sinai since the time of the most recent interglacial. They inferred these rates from elevations of a coral terrace, an assumed empirical relation between footwall uplift and throw, an estimated fault dip, and a direction of total slip inferred from the estimated direction of maximum stretching. Therefore, motion between Sinai and Nubia should not be neglected in estimates of the motion of Arabia relative to Nubia. We suspect that part of the prior motivation for neglecting the motion between Sinai and Nubia has been that data from the Red Sea have been too limited to obtain an accurate estimate of the angular velocity of Nubia relative to Arabia without including the data (mainly fault strikes) along the Dead Sea fault system. With our improved data set, an accurate angular velocity is obtained without using these data of doubtful tectonic relevance.

METHODS

Spreading rates

Only 11 of the 64 spreading rates were determined from data in original digital form because most of the magnetic profiles, including those of Roeser (1975) and Izzeldin (1987), are available to us only in analogue form. The analogue profiles were digitized from published figures, which were first photographically enlarged, by a factor of 2 for all profiles presented by Roeser (1975) and in Fig. 13 of Izzeldin (1987) and by a factor of 3 for the profiles in Fig. 11 of Izzeldin (1987).

Each observed magnetic profile is projected onto a great-circle tangent to the horizontal perpendicular to the spreading-ridge segment it crosses in the Red Sea. Strikes of spreading centres in the Red Sea are estimated from published GLORIA side-scan sonar data (Garfunkel *et al.* 1987). Each magnetic profile is interpolated at an equal interval using a cubic spline function, and the best-fitting straight line is removed. Each projected, interpolated and detrended profile is reduced to the North Pole by phase shifting it by an angle determined from the e ective inclination of the present and remanent magnetic field directions (Schouten & McCamy 1972). The inclinations and declinations of the present field are estimated from the International Geomagnetic Reference Field. The remanent inclination is calculated by assuming that the time-averaged geomagnetic field has been that of an axial geocentric dipole and that the palaeomagnetic pole has coincided with the present spin axis for the past 4 Myr. The spreading rate we seek is the average over the past 3.2 Myr, corresponding to the time interval since the middle of chron 2A. Crossings of anomaly 2A on both sides of the ridge are used to determine each spreading rate.

To obtain a higher level of precision of estimated spreading rates and to bring greater objectivity to the estimates of the rates, a simple automated method was developed for the interpretation of the magnetic anomaly profiles. First, anomaly

2A on each deskewed profile is identified on each side of the ridge and an approximate spreading rate is estimated by visual comparison with various synthetic magnetic anomaly profiles, which assume a transition width of zero and are constructed at rate increments of 1 mm yr^{-1}. Unsurprisingly, our initial guess was generally within 1 mm yr^{-1} of the rate ultimately found by the automated method.

Second, the goodness of fit of the synthetic anomaly to the observed anomaly is assessed using only the two anomaly 2A segments of the synthetic (Fig. 2), which are windowed with a boxcar function. For a given spreading rate, v, and o set, j, the average summed squared misfit, r, is given by

$$r = \frac{1}{N-1} \sum_{i=1}^{N} [M_{obs}(i) - M_{syn}(i+j, v)]^2, \quad (1)$$

where N is the number of points used in the comparison and M_{obs} and M_{syn} are observed and synthetic magnetic anomaly values, respectively. Anomaly 2A on both sides of the spreading centre are fitted simultaneously on a single profile. For a given spreading rate, the summed squared misfit is determined for many di erent o sets. Each observed profile is compared with 21 synthetic magnetic anomaly profiles that di er from one another by 0.1 mm yr^{-1} rate and range from 1 mm yr^{-1} per year less than the initial visually estimated spreading rate to 1 mm yr^{-1} more than the initial rate. The values of v and j that together gave the lowest value of r were assumed to be the best estimates of v and j.

Uncertainties in spreading rates and azimuths of earthquake slip vectors

Uncertainties in spreading rates are poorly understood and in prior work have been estimated subjectively (Chase 1978; Minster & Jordan 1978; DeMets *et al.* 1990). The dispersion of data about values calculated from a best-fitting model suggests that previously assigned errors have been overestimated, for example by an average factor of about 2 for global plate-motion model NUVEL-1 (DeMets *et al.* 1990). Here we estimate the uncertainties in rates from the dispersion of the rate data about the values calculated from two di erent parametrized models. In the first the rates are assumed to reflect the motion between rigid plates. The second is a purely descriptive model, with a Chebyshev polynomial being fitted to the spreading rates as a function of latitude. To apply the former model, one must decide how many rigid plates bound the Red Sea and where their boundaries are located. The latter model, as it is purely descriptive, can be fitted to all the rates without regard to plate boundaries.

A potential drawback to estimating errors only from the dispersion of the data is that we neglect possible systematic errors, which might be significant for profiles unavailable in digital form and therefore digitized from published figures. There may also be significant systematic errors due to tectonic causes, for example if the stretching between Arabia and Nubia is not localized at the spreading ridge in places where we assume that it is.

Standard errors of 25° and 30° were assigned to slip vectors from earthquakes with seismic moments exceeding 10^{25} dyn cm and between 10^{24} and 10^{25} dyn cm, respectively.

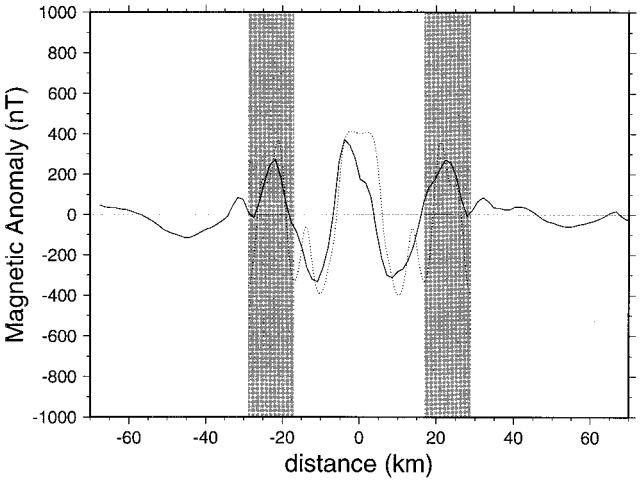

Figure 2. A best-fitting synthetic magnetic anomaly profile (dashed) is compared with an observed (solid) profile [profile 253 from Izzeldin (1982)], which has been reduced to the North Pole. The shaded regions show the portion of the anomaly 2A synthetic profile that is compared with the observed profile to determine the best-fitting spreading rate.

Timescale and spreading rates

Spreading rates were estimated using the timescale of Cande & Kent (1992). DeMets *et al.* (1994a) revised the NUVEL-1 set of angular velocities to bring them to consistency with the timescale of Hilgen (1991a,b). The resulting set of angular velocities, termed NUVEL-1 A, are merely those of NUVEL-1 multiplied by a scalar constant of 0.9562. For consistency with NUVEL-1A and other ongoing work that uses the Hilgen (1991a,b) timescale, here we convert all angular velocities to what they would have been if we had used the Hilgen (1991a,b) timescale instead of that of Cande & Kent (1992). For conversion from the Cande & Kent (1992) to the Hilgen (1991a,b) timescale the correction factor appropriate for the slow spreading rates we examine is 0.9956. Instead of directly correcting the spreading rates, we apply the correction to the angular velocities determined from the spreading rates. If we had instead corrected the individual spreading rates, the largest correction would be 0.1 mm yr^{-1}.

Linear formulation of inversion for angular velocities of relative plate motion

Because of the lack of useful transform fault azimuths, especially for spreading between the Danakil microplate and the Arabian Plate, the computer program we used in determining the NUVEL-1 global plate-motion model (DeMets *et al.* 1990) did not always successfully converge when applied to some of the small-spreading-rate data sets investigated herein. To explore these numerical di culties and to gain a better understanding of the structure of the errors in the data, it would be helpful to use singular value decomposition (SVD) in the inversion. Unfortunately, SVD can be applied only to a linear problem, and not to the non-linear azimuth functions used in the studies of Chase (1978), Minster & Jordan (1978) and DeMets *et al.* (1990). Instead, we used a linear formulation proposed by Simpson (1980).

Let ω, $\hat{\mathbf{t}}_\perp$ and $\hat{\mathbf{r}}$, respectively, be the angular velocity of one plate relative to another, the horizontal unit vector perpendicular to a transform fault, and the unit vector parallel to the site location (that is, the vector from the origin to the site). The component of velocity perpendicular to a transform fault should be zero, i.e. $(\omega \times \hat{\mathbf{r}}) \cdot \hat{\mathbf{t}}_\perp = 0$ (Simpson 1980). The transform-fault-perpendicular component of velocity is in units of radians or degrees per million years and must be converted to kilometres per million years, which is equivalent to millimetres per year. Let the transform-fault-parallel direction unit vector be denoted as $\hat{\mathbf{t}}_\parallel$. From vector identities, it follows that

$$\omega \cdot \hat{\mathbf{t}}_\parallel = 0. \tag{2}$$

Let v be defined as the spreading rate measured in the ridge-perpendicular direction and $\mathbf{s}_\parallel$ be a unit vector in the horizontal ridge-parallel direction. Similarly, it follows that

$$\omega \cdot \hat{\mathbf{s}}_\parallel = v \tag{3}$$

(Simpson 1980). Again this equation predicts the ridge-perpendicular component of velocity in radians or degrees per million years and must be converted to kilometres per million years for comparison with observed spreading rates. Let the uncertainty of a transform fault azimuth be σ_θ (expressed in radians), and the uncertainty of a spreading rate be σ_v (expressed in kilometres per million years). Equations of the form of eqs (2) and (3) are weighted before they are combined in an inversion. In prior work azimuth data have typically been weighted by $1/\sigma_\theta$ and spreading rate data have in most cases been weighted by $1/\sigma_v$, which leads to a maximum likelihood estimate of the angular velocity (Minster *et al.* 1974).

Here we continue to weight spreading rates by $1/\sigma_v$. To weight the azimuth data in an analogous manner is less straightforward when using the linear formulation for azimuth data. The di culty is that the right-hand side of eq. (2), like that of eq. (3), is not a direction but a rate. The misfit to eq. (2) has the form $v \sin \beta$, where v is the rate of motion calculated from a trial value for angular velocity and β is the angle between the observed transform azimuth and the direction of motion calculated from the trial angular velocity. Thus we weight eq. (2) by $1/(v_t \sigma_\theta)$, where v_t is a trial value for the rate of plate motion along the transform fault. Because it is unlikely that we will precisely guess the right value for v_t *a priori*, this weighting requires that the inversion, although linear, be iterated. In each but the first iteration, v_t is replaced by the value calculated from the best-fitting angular velocity from the preceding iteration. Iteration is terminated if every component of angular velocity changes by less than 1.5×10^{-7} radians per million years. Whatever initial value was used (e.g. initial $v_t = 0.1, 1, 10$), convergence to the same final values was always obtained with five iterations or fewer.

Thus eq. (3) is weighted identically to that used by DeMets *et al.* (1990) and eq. (2) is weighted similarly to that used by DeMets *et al.* (1990). Similar errors and angular velocities were found by the two methods when the data gave useful constraints on all three components of angular velocity.

Confidence regions for angular velocities

Confidence regions were determined by linear propagation of errors from the data to a covariance matrix that describes the uncertainty of one or more angular velocities. Confidence regions di er here, however, from those of prior work in two ways. First, the covariance matrix and least-squares solution are found by SVD. SVD is more robust than some alternatives, in particular the solution of the normal equations by Gauss–Jordan elimination and the determination of the covariance matrix by inverting the curvature matrix, as were used by DeMets *et al.* (1990). The potential advantage of SVD for plate-motion inversions is its numerical stability when one or more components of the angular velocity are poorly constrained, as might be expected for small data sets that contain spreading rates but lack azimuthal data. When all components of angular velocity are well constrained, the covariance matrices found by Gauss–Jordan elimination and SVD were practically identical.

Second, we project confidence regions onto the Earth's surface in a manner di erent to that of DeMets *et al.* (1990), who used the procedure of Minster *et al.* (1974), as follows. A 3×3 angular velocity covariance matrix (σ) is written in a coordinate system in which one coordinate axis parallels the angular velocity, a second is parallel to local north, and the third is parallel to local east. A 2×2 submatrix, which corresponds to the north and east coordinate axes and is extracted from the 3×3 matrix, defines an ellipse of uncertainty in the plane tangent to the Earth's surface at the pole of rotation. Multiplying the principal axes of this ellipse by 2.45 gives a 95 per cent confidence region for the pole, which has mirror symmetry in planes perpendicular to both principal axes of the ellipse. DeMets *et al.* (1990) projected these planar ellipses radially onto the Earth's surface, which then gives a confidence region with the same mirror symmetries as the planar ellipse.

Here we find the boundary of the 3-D ellipsoid corresponding to a constant χ^2 surface of 5.99, which is the value for a 2-D 95 per cent confidence region. This ellipsoid is projected radially onto the Earth's surface, resulting in general in an asymmetric 2-D confidence region that more accurately reflects the true confidence region for the pole of rotation. An asymmetry results, for example when the longest axis of the 3-D confidence region has both a significant radial component and a significant tangent plane component. In this case the projected confidence region is larger for the downward-dipping portion of the confidence ellipsoid relative to the upward-dipping side of the confidence ellipsoid.

The angular speed is $\omega = (\omega_x^2 + \omega_y^2 + \omega_z^2)^{1/2}$. Its standard error is found by linear error propagation from $\sigma_\omega^2 = \hat{\omega}^{\mathrm{T}} \sigma^2 \hat{\omega}$, where $\hat{\omega}$ is a unit vector parallel to ω. Similarly, from eq. (3), the standard error on calculated (or predicted) velocity at the ridge-perpendicular direction on the site (λ, ϕ) is $\sigma_v^2 = \hat{\mathbf{s}}_\parallel^{\mathrm{T}} \sigma^2 \hat{\mathbf{s}}_\parallel$, where $\hat{\mathbf{s}}_\parallel$ is the horizontal ridge-parallel unit vector. In local Cartesian coordinates, the components of velocity can be written as $v_{\mathrm{n}} = \omega_x \sin \phi - \omega_y \cos \phi$, $v_{\mathrm{e}} = \omega_z \cos \lambda - (\omega_x \sin \lambda \cos \phi + \omega_y \sin \lambda \sin \phi)$ and $v_{\mathrm{d}} = 0$. The speed, v, and azimuth, θ, of the velocity are obtained from these expressions. The standard deviation of the azimuth (σ_θ) is determined from linear propagation of errors, i.e.

$$\sigma_\theta = (a_x^2 \sigma_x^2 + a_y^2 \sigma_y^2 + a_z^2 \sigma_z^2 + a_x a_y \sigma_{xy} + a_x a_z \sigma_{xz} + a_y a_z \sigma_{yz})^{1/2} v^2, \tag{4}$$

where $a_x = \omega_y \sin \lambda - \omega_z \cos \lambda \sin \phi$, $a_y = \omega_z \cos \lambda \cos \phi - \omega_x \sin \lambda$ and $a_z = \cos \lambda v_{\mathrm{n}}$.

Test for additional plate boundaries

Procedures similar to those of DeMets *et al.* (1994b) and Gordon *et al.* (1987) are used to determine whether the addition of a Danakil microplate significantly improves the fit to the data. To locate the triple junction, we take the latitude corresponding to the lowest value of χ^2 as the best estimate of its location along the spreading centre. Confidence limits on its location are found from the following statistic: $\Delta\chi^2 = \chi^2(6) - \chi^2\,\text{min}$, where $\chi^2(6)$ is the sum squared normalized misfit for a hypothetical triple-junction latitude and $\chi^2\,\text{min}$ is the lowest sum squared normalized misfit among all hypothetical latitudes. This statistic is expected to be chi-square distributed with 1 degree of freedom.

DATA AND RESULTS

Magnetic anomaly profiles and spreading rates

Spreading rates are estimated from shipboard and aeroplane magnetic anomaly profiles (Fig. 3, Table 1). We used three sources for magnetic anomaly profiles: (1) 11 shipboard profiles collected in 1971 and 1979 and archived at the National Geophysical Data Center; (2) 28 aeromagnetic anomaly profiles from a 1976 survey (Izzeldin 1987); and (3) 25 magnetic anomaly profiles from the 1971 R/V *Valdivia* shipboard survey (Roeser 1975). Each de-skewed observed magnetic anomaly profile is compared with its best-fitting synthetic (Fig. 4).

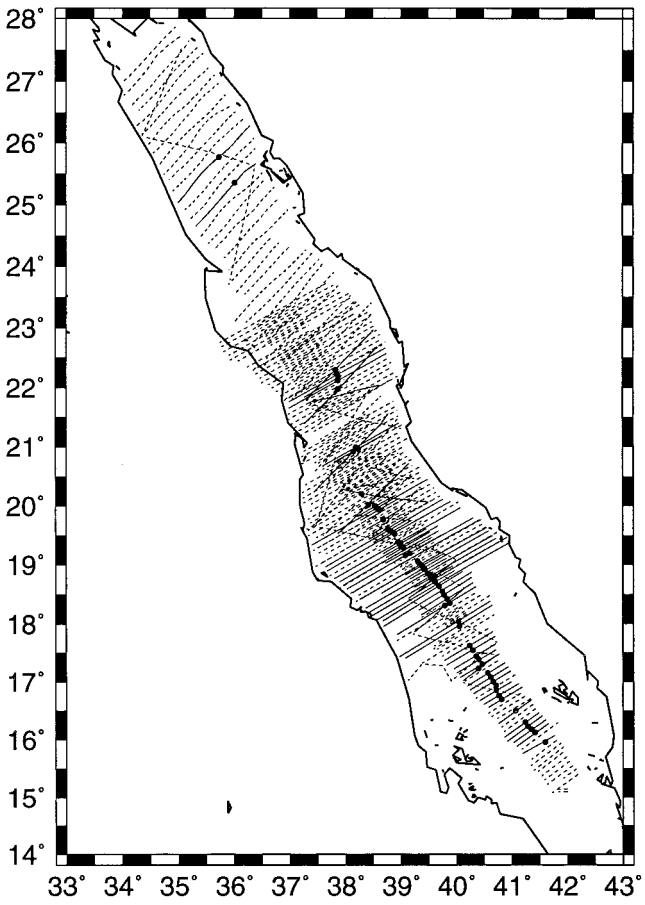

Figure 3. Locations of magnetic profiles in the Red Sea. The solid lines are the profiles from which spreading rates are obtained. The dashed lines are the other profiles investigated.

Southern Red Sea (15°–18.6°N)

This region is sampled mainly by the profiles of Roeser (1975), 55 of which cross the ridge and are oriented nearly perpendicular to the ridge; from these we were able to determine 25 spreading rates. The anomaly that Roeser (1975) labelled as 3 Ma is anomaly 2A. We were able to newly identify anomaly 2A from seven profiles, R04, R06, R08, R10, R12, R20 and R22, which were previously uninterpreted (Fig. 4). These new identifications correlate well with adjacent profiles from Izzeldin (1987) and the NGDC. Profile 30, which was interpreted by Roeser (1975) and DeMets *et al.* (1990), was discarded here. We now think that this profile probably crosses a transform fault (or fracture zone) because it does not correlate with adjacent profiles. Three additional rates were obtained from *Chain*-71 profiles (C3, C14 and C16 in Fig. 4), which are oriented nearly perpendicular to the ridge and have clear crossings of anomaly 2A.

Central Red Sea (18.6°–23°N)

There are 127 aeromagnetic profiles shown by Izzeldin (1982, 1987), all striking N60°E. We digitized 55 of these profiles. The rest of the profiles were unused either because some profiles were too close to one another to distinguish them or because the amplitude of the magnetic anomaly was too small to digitize reliably. Our identifications of anomaly 2A agree with those of Izzeldin (1982, 1987). Four spreading rates from the seven profiles from RRS *Shackleton* 1979 are located in the northern portion of this region. These profiles are orientated N45°E, which is nearly perpendicular to the ridge. Although anomaly 2A is not very clear, our identifications are similar to those of Girdler & Southren (1987) and correlate well with those from adjacent profiles. Many other profiles obtained from the NGDC cross the ridge in this region. Unfortunately we were able to estimate only two rates from these profiles because of the large spacing between samples, the large angle between most profiles and the ridge-perpendicular direction, or the failure of a profile to cross anomaly 2A on both sides of the ridge (Table 1, Fig. 4).

Northern Red Sea (23°–29°N)

After examining all profiles available from this region, we estimated spreading rates from only two. Although previous workers interpreted spreading rates from profiles as far north as 24°N (Izzeldin 1987; LaBrecque & Zitellini 1985; DeMets *et al.* 1990), most of these profiles have no distinctive central anomaly and we were unable to identify anomaly 2A convincingly. We were, however, able to identify anomaly 2A on profiles across Mabahiss Deep (25°–26°N) from four RRS *Shackleton* 1979 ridge crossings and one *Jean Charcot* 1978 crossing. Coutelle *et al.* (1991) and Guennoc *et al.* (1988) identified central and 2A anomalies at the same latitude with magnetic profiles from French cruises, most of which were unavailable to us. Two profiles give useful spreading rates, 9.7 mm yr^{-1} for the RRS *Shackleton* 1979 crossing b4 and 10.0 mm yr^{-1} for crossing b7. Given that these rates are slower

Table 1. Red Sea plate-motion data.

Lat. °N	Lon. °E	Datum	σ	Model	l	Ridge strike	Source or reference
Arabia–Nubia: spreading rates							
25.77	35.73	9.7	1.6	9.2	0.156	S40°E	*Shackleton* 1979, Prof. b4, NGDC
25.36	36.02	10.0	1.6	9.6	0.135	S40°E	*Shackleton* 1979, Prof. b7, NGDC
22.22	37.86	13.6	0.8	12.3	0.123	S40°E	Girdler & Southren (1987) Prof. d6
22.19	37.89	10.8	0.8	12.3	0.120	S40°E	Izzeldin (1987), profile 81
22.16	37.91	11.8	0.8	12.3	0.117	S40°E	Izzeldin (1987), profile 83
22.13	37.97	12.7	0.8	12.4	0.113	S40°E	Izzeldin (1987), profile 85
21.92	37.86	12.4	0.8	11.0	0.170	S21°E	Girdler & Southren (1987) Prof. d7
20.96	38.19	11.0	0.8	11.8	0.156	S21°E	Izzeldin (1987), profile 137
20.94	38.23	11.6	0.8	11.8	0.156	S21°E	Izzeldin (1987), profile 139
20.87	38.10	12.6	0.8	11.8	0.157	S21°E	Girdler & Southren (1987) Prof. d9
20.21	38.29	12.2	0.8	12.3	0.164	S21°E	*Chain* 1971, NGDC
20.02	38.42	13.8	0.8	13.5	0.040	S33°E	Girdler & Southren (1987) Prof. e2
20.00	38.53	12.6	0.8	13.5	0.040	S33°E	Izzeldin (1987), profile 181
19.97	38.56	12.0	0.8	13.6	0.040	S33°E	Izzeldin (1987), profile 183
19.94	38.61	13.2	0.8	13.6	0.040	S33°E	Izzeldin (1987), profile 185
19.77	38.68	13.6	0.8	14.1	0.038	S44°E	Izzeldin (1987), profile 193
19.61	38.77	13.8	0.8	14.3	0.035	S44°E	Izzeldin (1987), profile 201
19.58	38.81	13.0	0.8	14.3	0.035	S44°E	Izzeldin (1987), profile 203
19.55	38.86	14.7	0.8	14.4	0.034	S44°E	Izzeldin (1987), profile 205
19.52	38.89	15.0	0.8	14.4	0.034	S44°E	Izzeldin (1987), profile 207
19.39	38.95	14.0	0.8	14.5	0.033	S44°E	Izzeldin (1987), profile 213
19.36	38.99	14.6	0.8	14.5	0.033	S44°E	Izzeldin (1987), profile 215
19.31	39.00	14.8	0.8	14.6	0.032	S44°E	Izzeldin (1987), profile 217
19.28	39.05	15.0	0.8	14.6	0.032	S44°E	Izzeldin (1987), profile 219
19.19	39.16	14.8	0.8	14.7	0.032	S44°E	Izzeldin (1987), profile 225
19.16	39.08	15.2	0.8	14.7	0.032	S44°E	*Chain* 1971, NGDC
19.06	39.30	15.2	0.8	14.8	0.033	S44°E	Izzeldin (1987), profile 233
19.02	39.33	15.3	0.8	14.9	0.033	S44°E	Izzeldin (1987), profile 235
18.99	39.37	15.6	0.8	14.9	0.034	S44°E	Izzeldin (1987), profile 237
18.95	39.40	14.6	0.8	14.9	0.034	S44°E	Izzeldin (1987), profile 239
18.92	39.43	15.4	0.8	15.0	0.035	S44°E	Izzeldin (1987), profile 241
18.85	39.48	15.2	0.8	15.0	0.036	S44°E	Izzeldin (1987), profile 245
18.82	39.53	15.4	0.8	15.1	0.037	S44°E	Izzeldin (1987), profile 247
18.80	39.62	15.0	0.8	15.1	0.038	S44°E	*Chain* 1971, NGDC
18.78	39.55	15.0	0.8	15.1	0.037	S44°E	Izzeldin (1987), profile 249
18.74	39.59	15.2	0.8	15.1	0.038	S44°E	Izzeldin (1987), profile 251
18.71	39.62	14.8	0.8	15.2	0.039	S44°E	Izzeldin (1987), profile 253
18.63	39.69	15.4	0.8	15.3	0.041	S44°E	Roeser (1975), profile 04
18.55	39.75	15.2	0.8	15.3	0.043	S44°E	Roeser (1975), profile 06
18.48	39.78	15.5	0.8	15.4	0.045	S44°E	Roeser (1975), profile 08
18.42	39.83	15.5	0.8	15.4	0.047	S44°E	Roeser (1975), profile 10
18.35	39.88	16.1	0.8	15.3	0.072	S36°E	Roeser (1975), profile 12
18.31	39.79	15.2	0.8	15.3	0.071	S36°E	*Chain* 1971, NGDC
18.04	40.04	14.8	0.8	15.5	0.090	S36°E	Roeser (1975), profile 20
17.96	40.06	15.9	0.8	15.6	0.094	S36°E	Roeser (1975), profile 22

than any estimated for global plate-motion model NUVEL-1 (where the slowest spreading rates are 12 mm yr^{-1}, as observed along the Arctic Ridge), we interpret them with caution.

Slip vectors

No strike-slip focal mechanisms were found for the Red Sea between 17.6°N and 30°N, but five strike-slip mechanisms were found from the Harvard Centroid Moment Tensor (CMT) catalogue for the southernmost Red Sea (Fig. 5) near the boundaries of the Danakil microplate. Only the earthquake of 1988 December 10 is located near the spreading ridge. One possible slip vector has an azimuth of approximately N70°E, nearly orthogonal to the strike of the spreading ridge, and the other is nearly parallel to the ridge. We assume the former direction is the actual slip vector and that it reflects motion between the Arabian Plate and the Danakil microplate.

The other four earthquakes are located o the ridge in the zone of seismicity that branches southwestwards from the ridge as part of the boundary between the Nubian Plate and the Danakil microplate (Fig. 5). That a line drawn through the four events strikes about the same as the ≈N20°E azimuth of the slip vector corresponding to left-lateral slip suggests, but by no means proves, that this is the correct direction of slip.

Table 1. (*Continued.*)

Lat. °N	Lon. °E	Datum	σ	Model	l	Ridge strike	Source or reference
Arabia–Danakil: spreading rates							
17.62	40.24	14.8	0.8	15.2	0.165	S36°E	Roeser (1975), profile 32
17.54	40.30	15.4	0.8	15.1	0.142	S36°E	Roeser (1975), profile 34
17.44	40.36	14.0	0.8	14.9	0.119	S36°E	Roeser (1975), profile 40
17.38	40.41	14.6	0.8	14.8	0.106	S36°E	Roeser (1975), profile 42
17.30	40.47	14.2	0.8	14.6	0.091	S36°E	Roeser (1975), profile 44
17.23	40.40	13.6	0.8	14.6	0.088	S36°E	*Chain* 1971, NGDC
17.15	40.57	14.2	0.8	14.3	0.070	S36°E	Roeser (1975), profile 48
17.08	40.62	13.4	0.8	14.2	0.063	S36°E	Roeser (1975), profile 50
17.00	40.67	15.2	0.8	14.0	0.057	S36°E	Roeser (1975), profile 52
16.93	40.72	15.0	0.8	13.9	0.054	S36°E	Roeser (1975), profile 54
16.85	40.72	15.6	0.8	13.8	0.053	S36°E	Roeser (1975), profile 56
16.76	40.77	13.4	0.8	13.6	0.053	S36°E	Roeser (1975), profile 58
16.69	40.82	14.6	0.8	13.4	0.056	S36°E	Roeser (1975), profile 60
16.50	41.07	12.4	0.8	13.0	0.078	S36°E	Roeser (1975), profile 74
16.30	41.24	13.2	0.8	12.5	0.117	S36°E	Roeser (1975), profile 80
16.23	41.29	10.8	0.8	12.4	0.133	S36°E	Roeser (1975), profile 81
16.18	41.35	12.6	0.8	12.3	0.149	S36°E	Roeser (1975), profile 82
16.12	41.42	12.4	0.8	12.1	0.170	S36°E	Roeser (1975), profile 83
15.95	41.60	10.8	0.8	11.7	0.236	S36°E	Roeser (1975), profile 92
Arabia–Danakil: slip vectors							
16.33	41.08	69.2	30.0	69.4	0.373		CMT, 12.10.1988
Nubia–Danakil: slip vectors							
16.66	40.28	102.3/17.0	25.0	−8.6	–		CMT, 12.28.1977
16.52	40.26	102.0/12.0	30.0	−5.4	–		CMT, 01.17.1978
16.52	40.27	113.8/26.2	25.0	−5.3	–		CMT, 01.14.1980
16.45	40.23	121.0/21.0	30.0	−3.7	–		CMT, 01.14.1980

l is the data importance, a measure of the information content of a datum (Minster *et al.* 1974). σ is the standard error associated with a datum. Rates are in mm yr^{-1} and were estimated using the timescale of Cande & Kent (1992). Standard errors of spreading rates are estimated from the dispersion of the rates. Azimuths of relative motion are in degrees clockwise from north. 'NGDC' indicates a rate that was determined from data we obtained from the National Geophysical Data Center. Slip vectors labelled 'CMT' are from Harvard CMT solutions. The first and second directions of slip given for each Nubia–Danakil slip vector correspond, respectively, to right-lateral and left-lateral strike slip.

Below we invert these data for two alternative possibilities, the first corresponding to left-lateral slip for all four events and the second to right-lateral slip (with slip near S70°E) for all four events.

Dispersion of spreading rates

For all Red Sea rates combined and weighted equally, an F-ratio test showed that a fourth-order Chebyshev polynomial (i.e. one with five terms) fitted the data significantly better than did lower-order polynomials (Fig. 6) and gave a standard deviation of 0.77 mm yr^{-1} with a 95 per cent confidence interval of 0.65–0.94 mm yr^{-1}. The standard deviation was 0.74 mm yr^{-1} with a 95 per cent confidence interval of 0.63–0.91 mm yr^{-1} when the rates were fitted as if they recorded spreading between rigid plates (i.e. for a model with three rigid plates, Arabia, Nubia and Danakil, as discussed below).

Some profiles obviously record seafloor spreading and geomagnetic reversals with higher fidelity than others. The clearest profiles were 12 adjacent profiles from 18.74° to 19.19°N (Table 1, Fig. 4). These 12 data have a standard deviation about their mean value of only 0.27 mm yr^{-1} with a 95 per cent confidence interval for that standard deviation of 0.19–0.46 mm yr^{-1}. In contrast, the other 52 rates have a standard deviation about a Chebyshev polynomial fit of 0.82 mm yr^{-1} with a 95 per cent confidence interval of 0.68–1.02 mm yr^{-1}. If the two northernmost rates are omitted the standard deviation shrinks to 0.76 mm yr^{-1} with a 95 per cent confidence interval of 0.63–0.96 mm yr^{-1}. Thus, the standard deviation of the 12 best rates is significantly smaller than that of the remaining data whether or not the two northernmost rates are excluded. We choose to assign errors conservatively, however, using an assigned uncertainty of 0.8 mm yr^{-1} for all but the two northernmost rates, which are assigned larger uncertainties of 1.6 mm yr^{-1}.

Location of the Arabia–Danakil–Nubia triple junction

If, as previous analyses suggest, the pole of rotation between Arabia and Nubia is located $\approx 15°$ NNW of the north end of the Red Sea, the spreading rate should monotonically increase to the SSE. Instead, the spreading rate reaches its maximum near 18°N, declines both north and south of there, and cannot be fitted as spreading between a single pair of rigid plates (Fig. 6). At least part of the decrease to the south or to the north or to both must be caused by stretching of the crust not localized at the spreading ridge. A simple and useful model for

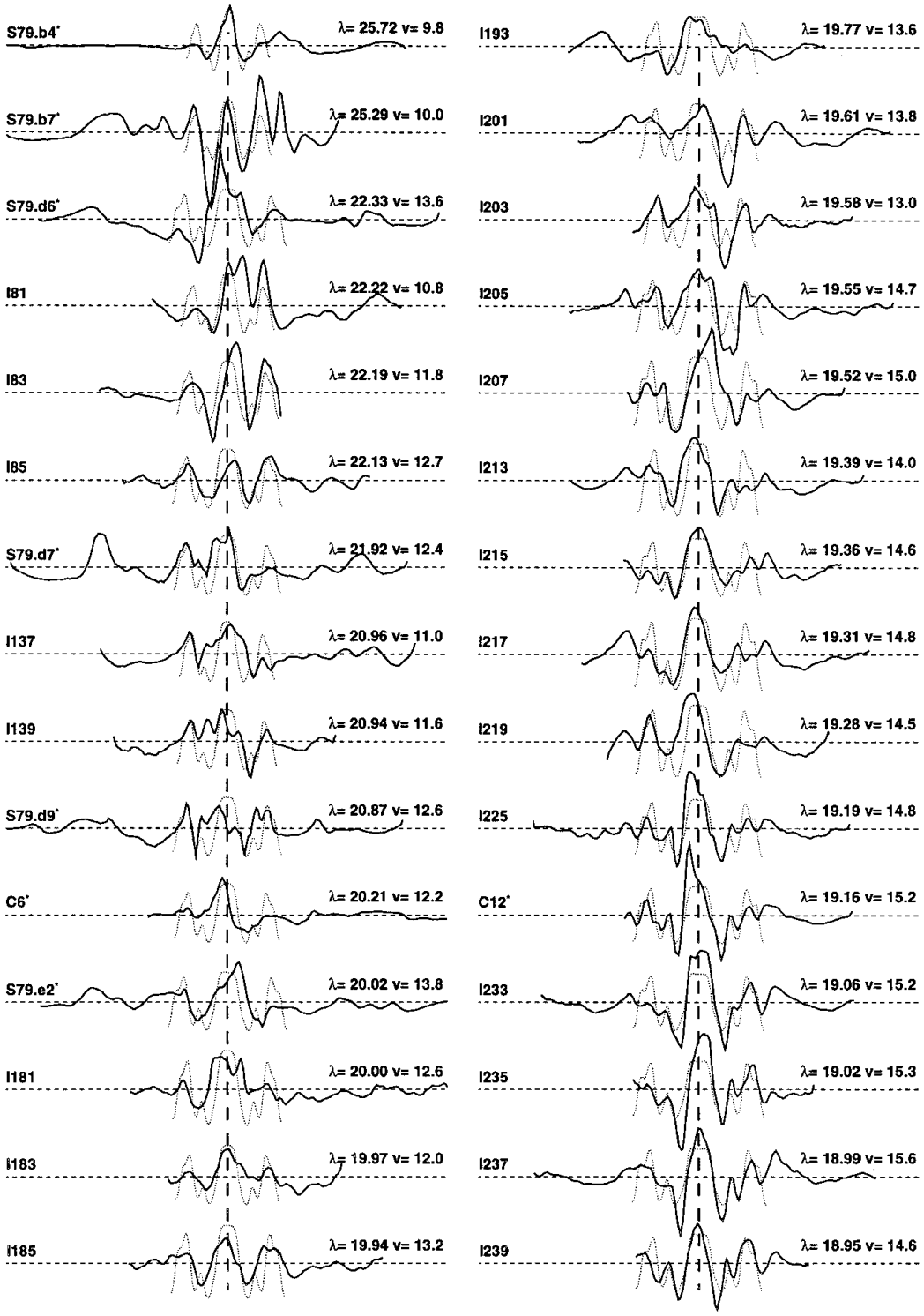

Figure 4. The magnetic profiles for the Red Sea. The solid curves are the magnetic anomaly profiles reduced to the North Pole. The dashed curves are the best-fit synthetic anomaly profiles. λ is the latitude of each profile where it crosses the ridge and v is the best-fitting full spreading rate in millimetres per year. Profile abbreviations: R, profiles from Roeser (1975); I, profiles from Izzeldin (1987); S79, RRS *Shackleton* 1979; C, *Chain* 1971. * indicates profiles obtained in original digital format.

this deformation is that a Danakil microplate exists between Nubia and Arabia west of the spreading centre in the southern Red Sea (Le Pichon & Francheteau 1978).

We used the plate-motion data to test for the significance of the motion of the Danakil microplate relative to Nubia and for the location of the triple junction between the Arabian Plate, the Nubian Plate and the Danakil microplate. The minimum value of χ^2 of 48.04 with 57 degrees of freedom, corresponding to a maximum value of F of 32.827 with 4 and 57 degrees of freedom, occurs in the interval

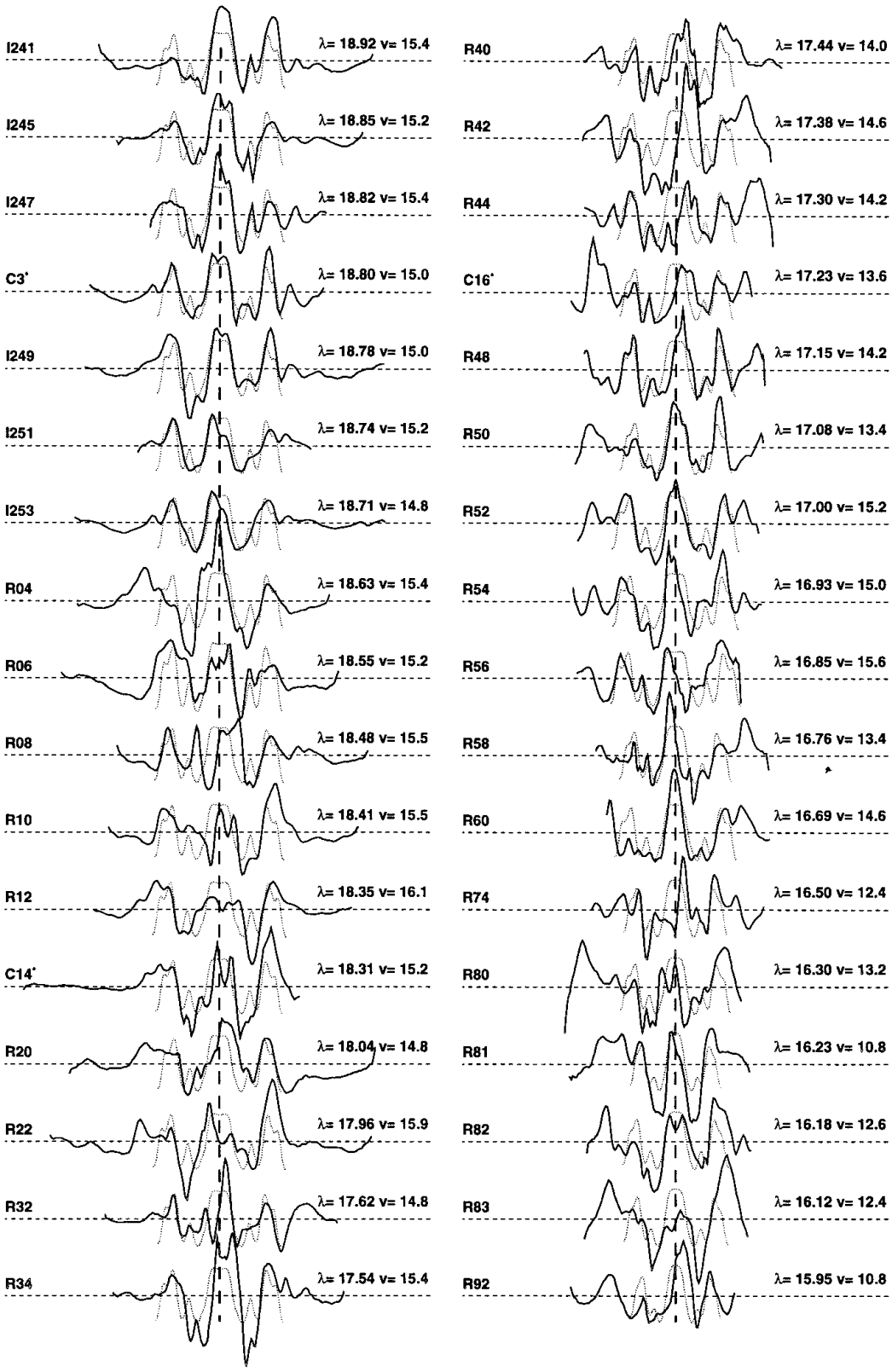

Figure 4. (*Continued.*)

18.04°–18.31°N; the probability of obtaining a value this large or larger by chance if all rates record Arabia–Nubia spreading is only 3.4×10^{-14}. The 95 per cent confidence limits are 17.4°–18.7°N (Fig. 7).

The western branch of seismicity merges with the Red Sea spreading ridge near 17.0°–17.5°N (Figs 1 and 5). The widest ridge trough is at about the same latitude, and the highest spreading rate is a little further north at ≈18.0°N. The gap

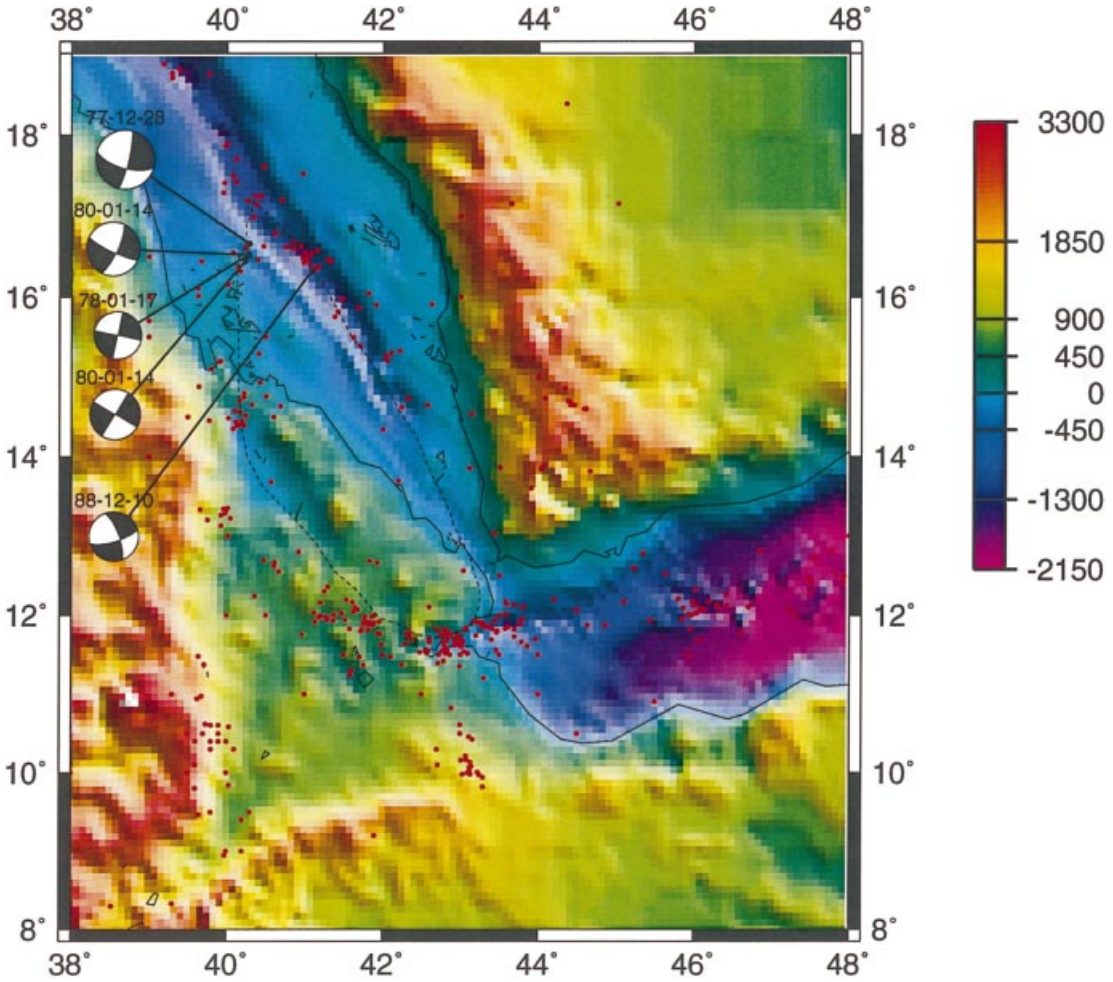

Figure 5. Centroid moment tensor solutions in the southern Red Sea from the Harvard catalogue (1976–1996) and topography in Afar and the southern Red Sea. The dots show epicentres of earthquakes from 1950 to 1993. The dashed line shows the approximate boundaries of the Danakil microplate. The 1988 December 10 earthquake is located near the spreading ridge and is assumed to result from the motion between the Danakil microplate and the Arabian Plate. The other four earthquakes were o -ridge earthquakes and were located in the zone that was assumed to be the boundary between the Danakil microplate and the Nubian Plate.

in spreading rates between 17.62 and 17.96°N lies within the 95 per cent confidence interval; it is convenient to assume that the triple junction is located in this gap.

Northern limit of correlatable magnetic anomalies due to seafloor spreading

The northern limit of regular sequences of magnetic anomalies is at ≈19.5°N (Izzeldin 1987). Aside from five profiles across the Mabahiss Deep (25°–26°N), the northernmost well-correlated crossings of anomaly 2A are near 22.4°N (Girdler & Southren 1987; Izzeldin 1987). The nature of crust north of 21°N is debatable (Girdler & Southren 1987; Cochran 1983). Girdler & Southren (1987) concluded that nearly all the seafloor north of 21°N formed by localized spreading like that at typical mid-ocean ridges. They attributed the low remanent magnetization to the cover of evaporites. Cochran (1983) argued that the post-Miocene sediments have a relatively constant thickness across the main trough north of 25°N. Moreover, gravity and magnetic anomalies suggest the presence of isolated intrusions. He concluded that extension is accommodated over a wide zone north of 25°N and that the region from 21° to 25°N is a transition zone between the localized spreading to the south and di use spreading to the north. O -ridge earthquakes and volcanoes are more prevalent north of ≈23°N than further south (Fig. 1), suggesting that Arabia–Nubia relative motion may be less well localized north of 23°N, which is consistent with the near absence of correlatable anomalies north of 23°N. For this reason, and because the inferred rates of seafloor spreading are so slow, we have interpreted the spreading rates from the Mabahiss Deep (25°–26°N) with caution. Thus, we first inverted the data without the two rates from the Mabahiss Deep. With this angular velocity, we predicted the rates for the Mabahiss Deep. The predicted rates are insignificantly slower than the observed rates (Fig. 6) and give no hint of significant motion not localized at the spreading centre at this latitude.

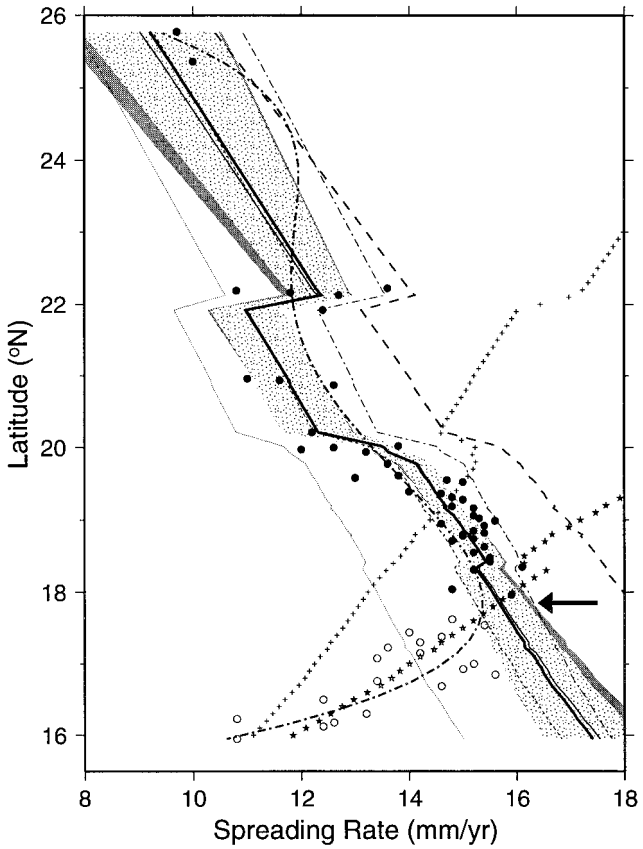

Figure 6. Observed Red Sea spreading rates (circles) are fitted by five terms (including a constant term) of a Chebyshev polynomial (thick dot–dashed curve) as a function of latitude. The arrow shows the location of the maximum spreading rate of the fitted curve. Six curves show the rates calculated from various estimates of the angular velocity of Arabia relative to Nubia: thick solid curve, angular velocity determined from rates north of 17.7°N (the heavily shaded region shows the 1σ uncertainty of these calculated rates); thin solid curve, angular velocity from rates north of 17.7°N and south of 23°N (the lightly shaded region shows the 1σ uncertainty of these calculated rates); long-dashed curve, best-fitting angular velocity of Jestin *et al.* (1994); dotted curve, that of Jo e & Garfunkel (1987); thin dot–dashed curve, that of Chase (1978); short-dashed curve, that of Le Pichon & Gaulier (1988). Two curves show the rates calculated from estimates of the angular velocity of Arabia relative to Danakil: stars, angular velocity determined from spreading rates south of 17.7°N (open circles) and from one earthquake slip vector from the southern Red Sea; plusses, angular velocity of Le Pichon & Francheteau (1978). All rates were rescaled for consistency with the timescale of Hilgen (1991a,b).

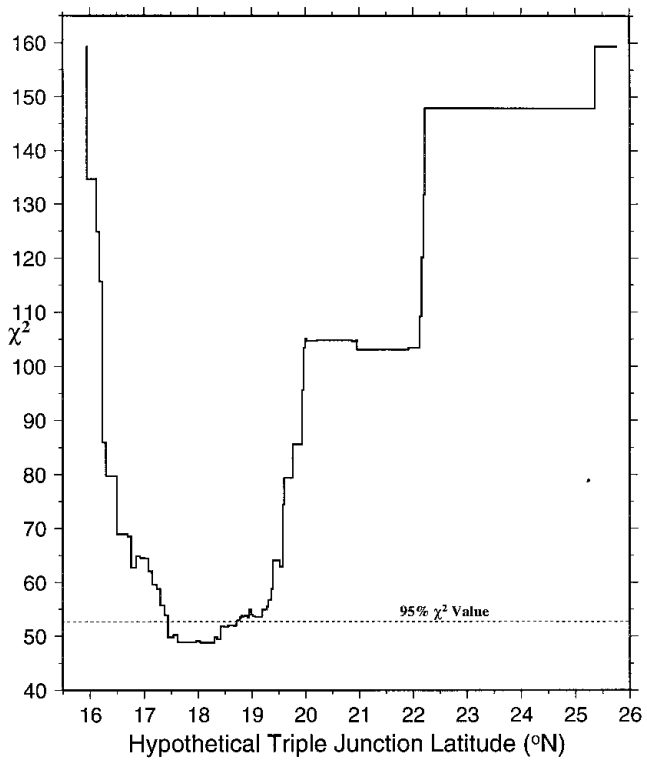

Figure 7. Chi-square values (summed squared normalized misfit) versus hypothetical latitudes of the Danakil–Arabia–Nubia triple junction. The dashed line is the threshold for the 95 per cent confidence limit for the location of the triple junction.

Angular velocity of Arabia relative to Nubia

The angular velocity of Arabia relative to Nubia is $0.403^\circ\ \mathrm{Myr}^{-1}$ about 31.5°N, 23.0°E (Table 2, Fig. 8). The chi-square value is 27.7 with 42 degrees of freedom; the probability of obtaining a value this small or smaller if the errors are correctly estimated is 4.3 per cent. Thus, we slightly overestimate the uncertainty of the angular velocity. Although the Arabia–Nubia poles of rotation of Jestin *et al.* (1994), Jo e & Garfunkel (1987), and Chase (1978) lie within the 95 per cent confidence region for our new pole of rotation (Fig. 8), the Arabia–Nubia angular velocities from these previous studies, except that of Le Pichon & Gaulier (1988), lie outside both the 95 and the 99 per cent confidence regions of our new angular velocity (Table 3). The volume of the confidence ellipsoid for the new angular velocity is smaller than found in previous studies, even those that also include data along the Dead Sea rift and transform azimuths from the Red Sea that we consider unreliable (Table 3).

It is useful to decompose the angular velocity into the three orthogonal directions defined by the eigenvectors of the covariance matrix (Fig. 9). The least uncertain component of angular velocity parallels the eigenvector that lies in eastern Canada; its value and 1σ uncertainty are $0.128 \pm 0.001^\circ\ \mathrm{Myr}^{-1}$ (Fig. 9). Its small uncertainty shows that the average spreading rate in the Red Sea is well constrained. The middling uncertain component of angular velocity parallels the eigenvector that lies in the south Atlantic; its value and 1σ uncertainty are $0.051 \pm 0.008^\circ\ \mathrm{Myr}^{-1}$, indicating a significant di erence from zero (Fig. 9). This uncertainty is surprisingly small because it is the component of angular velocity that one expects to be controlled by the non-existent azimuthal data. Thus it indicates that the direction of motion across the Red Sea is usefully constrained. The most uncertain component of angular velocity parallels the eigenvector that lies near the Arabian coast of the Red Sea; its value and 1σ uncertainty are $0.380 \pm 0.049^\circ\ \mathrm{Myr}^{-1}$, which also di ers significantly from zero (Fig. 9). That this component is positive indicates that the pole of rotation corresponding to a positive angular velocity lies between 0° and 90° from the Red Sea; that it is several times larger than the first component indicates that the pole of rotation lies closer to 0° than to 90° from the Red Sea (Fig. 9).

Table 2. Angular velocities and uncertainties.

Plate pair	Lat. °N	Lon. °E	ω ° Myr^{-1}	σ_x^2	σ_y^2	σ_z^2	σ_{xy}	σ_{xz}	σ_{yz}
				10^{-10} radians^2 Myr^{-2}					
Ar–Nb	31.5	23.0	0.403	3344	2889	1140	2978	1781	1795
Dk–Ar	8.9	43.9	0.854	38454	30927	10399	26225	10013	16900
Dk–Ar*	11.5	47.5	0.871	35958	26160	5968	29675	13339	12305
Dk–Ar†	9.9	45.2	0.860	35756	26006	5766	29847	13535	12127
Dk–Nb	16.3	37.9	1.220	41798	33816	11539	29203	11793	18695
Dk–Nb*	18.2	40.6	1.235	39253	28843	6926	32742	15206	13906
Dk–Nb†	17.0	38.9	1.227	39537	28001	6299	32800	15216	13177

Each angular velocity describes a right-handed rotation of the first plate relative to the second and is calculated using the timescale of Hilgen (1991a,b). Plate abbreviations: Ar, Arabia; Nb, Nubia; Dk, Danakil. The covariance matrix is described in Cartesian coordinates: x (0°N, 0°E); y (0°N, 90°E); z (90°N). *Four slip vectors from strike-slip earthquakes along the Nubia and Danakil boundary were included in the inverted data assuming that their slip was in the plane that is nearly perpendicular to the strike of the boundary. †Four slip vectors from strike-slip earthquakes along the Nubia and Danakil boundary were included in the inverted data assuming that their slip was in the plane that is nearly parallel to the strike of the boundary.

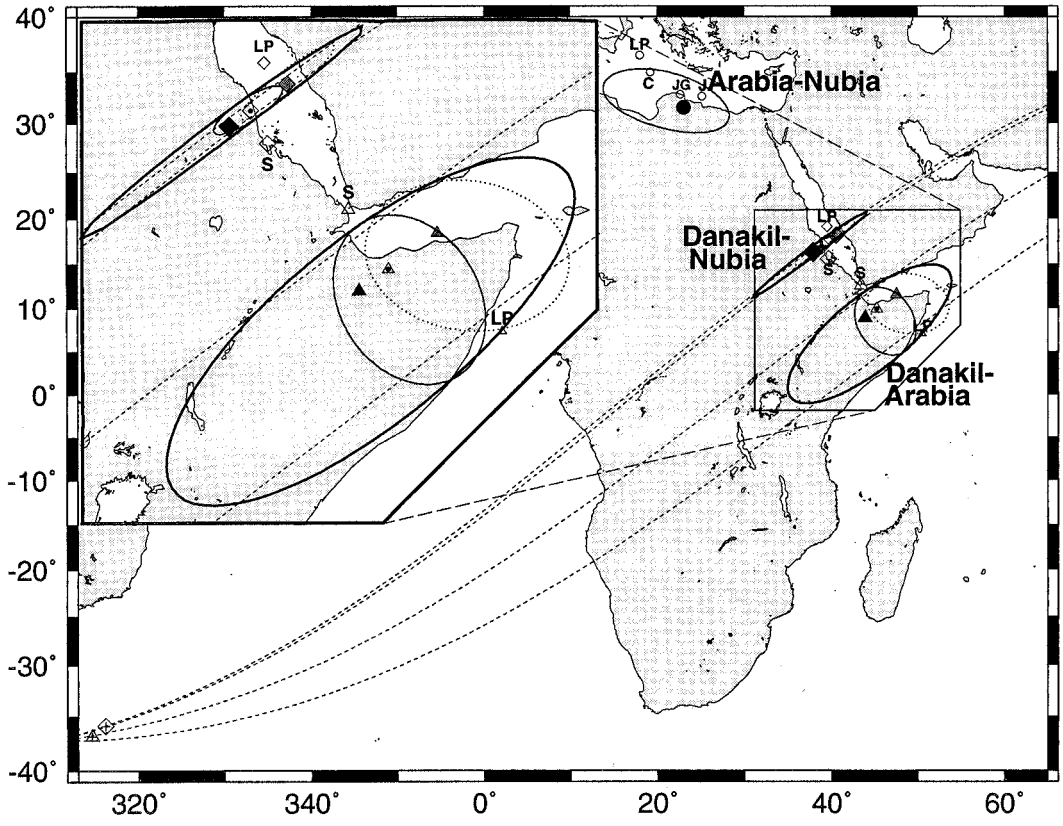

Figure 8. Poles of rotation and 95 per cent confidence limits. Poles for Arabia relative to Nubia are shown by circles, Danakil relative to Arabia by triangles, and Danakil relative to Nubia by diamonds. Previously published poles are shown as follows: J is the best-fitting angular velocity of Jestin *et al.* (1994); JG is that of Jo e & Garfunkel (1987); C is that of Chase (1978); LP is that of Le Pichon & Francheteau (1978); S is that of Sichler (1980). Our new preferred poles of rotation are shown by solid symbols; their 95 per cent confidence limits are shown by solid curves. The preferred pole for the southern Red Sea incorporates one earthquake slip vector. Alternative poles are shown as follows: plus sign inside symbol (dashed 95 per cent confidence region), no slip vectors were used to determine the angular velocity; stippled symbol (dotted 95 per cent confidence region), four Nubia–Danakil slip vectors were used assuming slip directions near N70°W; solid dot inside symbol (thin solid 95 per cent confidence region), four Nubia–Danakil slip vectors were used assuming slip directions near N20°E.

Angular velocity of Danakil relative to Arabia

The inversion of spreading rates south of 17.7°N gives a best-fitting angular velocity for Danakil relative to Arabia of 14.477° Myr^{-1} about a pole located at −36.9°N, −45.4°E, which lies close to the southwestern edge of the 95 per cent confidence region (Fig. 8). The chi-square value is 21.0 with 16 degrees of freedom; the probability of obtaining a value this large or larger if the errors are correctly estimated is 18 per cent. An F-ratio test comparing the dispersion of the rates north of 17.7°N with those south of 17.7°N indicates that the southern data are significantly more dispersed than the

Table 3. Goodness of fit of angular velocities to the data.

Pole of rotation		Original timescale		Hilgen timescale		Volume of 95%	Source
Lat. (°N)	Lon. (°E)	ω_0	$\Delta\chi^2_0$	ω_0	$\Delta\chi^2_0$	confidence region	
Nubia–Arabia							
31.5	23.0	0.421[a]	28.8	0.403	0.0	10	This study*
32.8	22.6	0.402	38.7	0.374	6.9	–	Le Pichon & Gaulier (1988)[1]
38.7	17.5	–	–	0.313	145.8	1014	Jestin *et al.* (1994) Red Sea only[2]
32.6	25.2	–	–	0.464	186.5	26	Jestin *et al.* (1994) Dead Sea plus Red Sea[2]
37.3	19.2	–	–	0.332	111.3	3780	Chase (1978) Red Sea only[2]
36.5	18.0	0.320	48.6	0.298	14.8	–	Le Pichon & Francheteau (1978)[1]
34.9	19.2	0.371	267.7	0.347	62.9	–	Chase (1978)
32.2	24.0	0.376	75.5	0.350	260.9	–	Jo e & Garfunkel (1987) [1]
32.6	25.1	0.499	574.5	0.477	316.2	–	Jestin *et al.* (1994) best fitting
Danakil–Arabia							
8.9	43.9	0.893[a]	11.7	0.854	0.0	347	This study*
9.9	45.2	–	–	0.860	0.1	96	This study§
11.5	47.5	–	–	0.871	1.1	120	This study†
7.0	50.5	0.500	19.5	0.465	80.8	–	Le Pichon & Francheteau (1978)[1]
Danakil–Nubia							
16.3	37.9	1.276[a]	0.2	1.220	0.0	772	This study*
17.0	38.9	–	–	1.227	0.2	174	This study§
18.2	40.6	–	–	1.235	1.1	251	This study†
19.1	39.5	0.770	19.9	0.716	18.6	–	Le Pichon & Francheteau (1978)[1]

The angular speeds (ω) are given in $^\circ$ Myr^{-1} and have been revised to consistency with the timescale of Hilgen (1991a,b). A result di ers significantly (at the 95 per cent confidence level) from the preferred result of this study if $\Delta\chi^2$ exceeds 7.82. The volume of the 3-D 95 per cent confidence region is in units of 10^{-12} radians^3. * Preferred result of this study, which is determined from spreading rates only for Nubia–Arabia motion, from spreading rates and one earthquake slip vector for Danakil–Arabia motion, and from vector summation of these first two angular velocities to determine Danakil–Nubia motion. § Slip vectors from four strike-slip earthquakes along the Nubia and Danakil boundary were also included in the inverted data; their slip was assumed to lie in the nodal plane that is nearly parallel to the strike of the boundary. † Slip vectors from the same four earthquakes were included assuming that their slip was in the nodal plane nearly perpendicular to the strike of the boundary. When all slip vectors are omitted the volumes increase to 58 522 and 127 408 for the Arabia–Danakil and Nubia–Danakil angular velocity, respectively, expressed in the same units as in the table. The Red Sea data of Jestin *et al.* (1994) include the azimuths of very short-o set transform faults, which we consider to be unreliable. [1] Timescale used in the cited paper is unclear. We assumed that it was the timescale of Talwani *et al.* (1971). [2] Found using our fitting program from the data of the cited source. [a] Results from this study converted to the timescale of Harland *et al.* (1982) to illustrate the e ect of the change in timescale.

northern data at the 95 per cent confidence level. With hindsight, it would therefore have been better to assign slightly smaller (19 per cent) uncertainties to the rates north of 17.7°N and slightly larger (14 per cent) uncertainties to the rates south of 17.7°N.

It is useful to consider the uncertainties of the three components of angular velocity parallel to the eigenvectors of the covariance matrix, which are located at 50.7°N, 289.0°E, 10.6°N, 32.3°E and 37.3°S, 310.4°E, similar to those found for motion between Arabia and Nubia (Fig. 9). The components of angular velocity along the first two directions are well constrained, but the third component, which lies in the western South Atlantic, is essentially unconstrained, being $-14.452 \pm 10.833^\circ$ Myr^{-1} (1σ). This poorly constrained component of angular velocity indicates a ridge-parallel component of velocity of Arabia relative to Danakil of 1600 ± 2400 mm yr^{-1} (95 per cent confidence limits) to the SSE. Unlike the case for the Arabia–Nubia angular velocity, this example thus fits our preconceived notion that in the absence of directional data, the ridge-parallel component of velocity is poorly constrained. In this case SVD is a useful tool for determining which components of angular velocity are well constrained and which are not. The projection of the corresponding 3-D ellipsoid onto the Earth's surface is well constrained in one direction and poorly constrained in the other (dashed confidence region in Fig. 8).

To improve the accuracy of the one unconstrained component of angular velocity, we next incorporated a slip vector from the earthquake near the spreading ridge of the southern Red Sea. Because of the absence of transform faults as long as or longer than 35 km, use of this datum is indefensible for any but a modest assumed accuracy. With the slip vector added, the best-fitting angular velocity for Danakil relative to Arabia is 0.854° Myr^{-1} about a pole located at 8.87°N, 43.90°E, which has a much smaller 95 per cent confidence region than does the angular velocity determined without the slip vector (Fig. 8). Incorporation of the one slip vector shrinks the volume of the confidence region by a factor of 169. The pole of Le Pichon & Francheteau (1978) lies within the 95 per cent confidence region of the new pole of rotation (Fig. 8), but the slower angular velocity found by Le Pichon & Francheteau (1978) lies outside both the 95 and the 99 per cent confidence ellipsoids for the new angular velocity (Table 3). Sichler (1980) proposed that the pole of rotation between the Danakil block and Arabian Plate is located at the southern limit of their mutual boundary. His pole lies outside the 95 per cent confidence limits of the new pole (Fig. 8), showing that his proposal is, at best, approximately correct.

With the slip vector incorporated, the component of angular velocity that parallels the eigenvector in the western South Atlantic (now located at 33.3°S, 325.5°E) equals $0.069 \pm 0.064^\circ$ Myr^{-1}. The ridge-parallel component of velocity

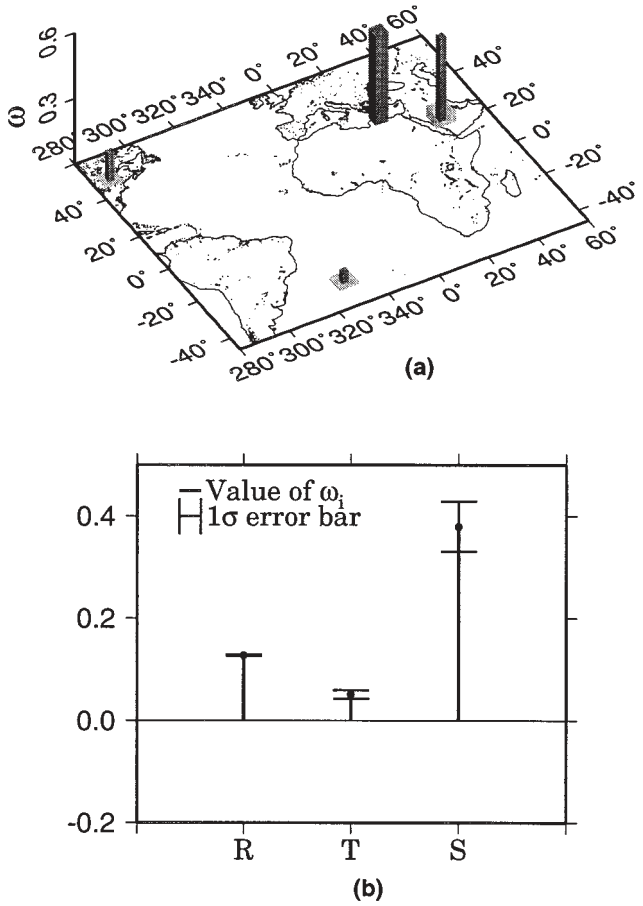

Figure 9. (a) The base of the largest rectangular prism (located in the eastern Mediterranean Sea) shows the location of the Arabia–Nubia pole of rotation. The height of the prism is proportional to the corresponding angular speed. The base of each of the other three rectangular prisms shows the location of an eigenvector of the covariance matrix of the Arabia–Nubia angular velocity. The height of each of these three prisms is proportional to the component of angular velocity parallel to the eigenvector. The lengths of these components are also shown in part (b), along with their 1σ uncertainties. The component labelled 'R' parallels the eigenvector in eastern North America, the component 'T' parallels the eigenvector in the South Atlantic Ocean, and the component 'S' parallels the eigenvector in Arabia.

of Arabia relative to Danakil in this case equals 4 ± 14 mm yr^{-1} (95 per cent confidence limits) to the NNW, which is consistent with orthogonal spreading but permits spreading to be up to $\approx 50°$ oblique. With the slip vector included, therefore, all three components of the angular velocity are usefully constrained and the projection of the corresponding 3-D ellipsoid onto the Earth's surface is well constrained in both directions (Fig. 8).

Angular velocity of Danakil relative to Nubia

The angular velocity of Danakil relative to Nubia was found by summing the Danakil–Arabia and Arabia–Nubia angular velocities, the former being that determined from both the southern Red Sea spreading rates and the one near-ridge earthquake slip vector. The resulting angular velocity is 1.220° Myr^{-1} about a pole at 16.29°N, 37.89°E. Unsurprisingly, the 3-D confidence region for the Nubia–Danakil angular velocity is larger than those for either of the two from which it was determined (Table 3). Perhaps surprisingly, the uncertainty region for the Danakil–Nubia pole of rotation is smaller than the uncertainty region for either the Arabia–Nubia or the Danakil–Arabia pole of rotation (Fig. 8). The smaller confidence region is mainly a consequence of the larger magnitude (1.220° Myr^{-1}) of the Danakil–Nubia angular velocity relative to those for Arabia–Danakil (0.854° Myr^{-1}) and Arabia–Nubia (0.420° Myr^{-1}). When the 3-D confidence ellipsoids are projected onto the Earth's surface, the Danakil–Nubia uncertainty region, being projected from a larger distance, maps onto a smaller area (Chang *et al.* 1990). When the uncertainty region is projected in the perpendicular direction, that is onto the 1-D rate of rotation, the 1σ uncertainty for Danakil–Nubia ($\pm 0.1565°$ Myr^{-1}) is, as expected, larger than the uncertainty for Arabia–Danakil ($\pm 0.1474°$ Myr^{-1}) and larger than the uncertainty for Nubia–Arabia ($\pm 0.0458°$ Myr^{-1}). The pole of rotation and the angular velocity for Nubia relative to Danakil of Le Pichon & Francheteau (1978) lie outside the 95 per cent confidence regions for our new pole of rotation (Fig. 8) and angular velocity (Table 3), respectively. Their pole of rotation lies to the north of the new pole of rotation and their angular velocity indicates that the separation rate of Nubia from Danakil is a few millimetres per year faster near the northern end of the Danakil–Nubia boundary than indicated by our angular velocity. Sichler (1980) proposed that Danakil is pinned to Nubia where his pole of rotation is located (Fig. 8). Our results show that this proposal is, at best, approximately correct; his pole of rotation lies south of the 95 per cent confidence limits of the new pole of rotation (Fig. 8). The new pole shows that relative motion, most likely to be a combination of stretching and left-lateral shearing, must be accommodated in the region that Sichler (1980) proposed to be pinned.

We also explored the use of slip vectors from the four earthquakes that have similar strike-slip mechanisms and lie along what is probably the Danakil–Nubia boundary (Fig. 5). We considered two possibilities: (1) that right-lateral slip occurred in all four events along $\approx$S70°E, and (2) that left-lateral slip occurred in all four events along $\approx$N20°E, which seems more likely. Both sets of slip vectors are consistent with the other plate-motion data, with the latter set being in slightly better agreement with the other data.

Strike of the spreading ridge and fracture zones

Spreading appears to di er insignificantly from orthogonality along the spreading-ridge segments in the central Red Sea (i.e. 18.4°–20°N), with significant obliquity north of 20°N (Fig. 10). Although there are no transform faults with o sets longer than 35 km, there are obvious transverse features that can be identified on the gravity map of Sandwell & Smith (1997) and that could be interpreted as short-o set fracture zones. The strikes of these fracture zones probably indicate the direction of relative motion across the Red Sea over an interval much longer than the 3 Myr considered here. The directions of motion indicated by the Arabia–Nubia angular velocity are CCW of the observed strikes of Red Sea fracture zones with the di erence north of 22°N being statistically significant (Fig. 10).

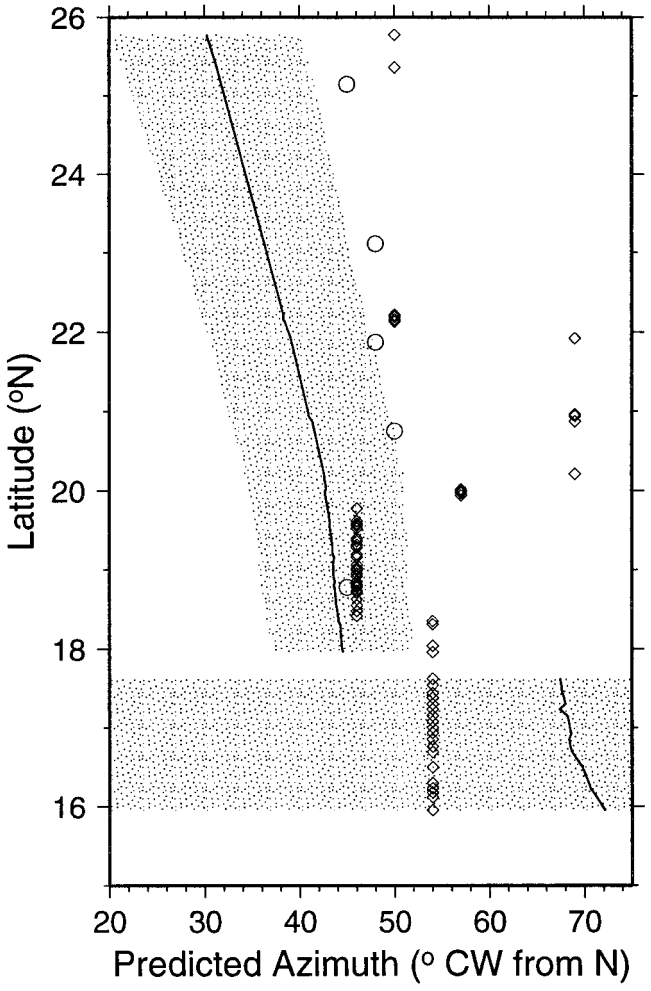

Figure 10. Predicted direction of motion (solid curve) and its 95 per cent confidence limit (shaded area) compared with the azimuths of fracture zones (open circles) estimated from gridded gravity data and with the direction normal to the ridge (open diamonds).

CONCLUSIONS

(1) The standard deviation of spreading rates in the Red Sea is ≈ 0.8 mm yr^{-1}, which is many times smaller than the errors typically assigned to spreading rates in previous work (for example, 4 mm yr^{-1} is the median error assigned to spreading rates in global plate-motion model NUVEL-1).

(2) An internally consistent set of correlations of the central anomaly and of anomaly 2A in the Red Sea can be made from 16° to 22.5°N, as well as on some additional profiles between 25° and 26°N. These rates range from a low of ≈ 10 mm yr^{-1} in the northern (26°N) Red Sea to a high of ≈ 16 mm yr^{-1} near 18°N.

(3) No transform faults in the Red Sea are long enough to give a reliable azimuth of the direction of relative plate motions.

(4) Rates in the Red Sea are fitted significantly better by two angular velocities than by one. The angular velocity of Arabia relative to Nubia is determined from rates north of ≈ 18°N and the angular velocity of Arabia relative to Danakil is determined from data south of ≈ 18°N. The 95 per cent confidence interval on the latitude of the Arabia–Danakil–Nubia triple junction, if the Danakil–Nubia boundary is narrow, are 17.4°–18.7°N. South of this boundary, the spreading rates decrease rapidly and are slower than predicted by the Arabia–Nubia angular velocity.

(5) The locations of earthquakes suggest that the localization of Arabia–Nubia motion to the Red Sea spreading ridge ceases south of ≈ 17.5°N, consistent with the division into two domains indicated by the spreading rates.

(6) Despite the absence of any reliable directional data, the angular velocity of Arabia relative to Nubia can be determined with useful accuracy from the available spreading rates. The confidence limits are compact and the direction of relative motion is determined with an accuracy of ± 8° (95 per cent confidence limits). In future work it should be possible to combine this angular velocity with that between Arabia and Somalia, as determined from data along the Sheba Ridge in the Gulf of Aden, to estimate the angular velocity of Nubia relative to Somalia with improved accuracy.

(7) The confidence limits for the angular velocity of Arabia relative to Nubia are much smaller than found by Chase (1978) or Jestin *et al.* (1994) (Table 3), which is unsurprising since only four spreading rates were used in the former study and two in the latter, many fewer than the 45 rates used here. The best-fitting angular velocities of Arabia relative to Nubia estimated by Le Pichon & Francheteau (1978), Chase (1978), Jo e & Garfunkel (1987), and Jestin *et al.* (1994) all lie outside the compact 3-D 95 per cent confidence region determined here.

(8) The 19 Red Sea spreading rates from profiles south of those interpreted as recording Arabia–Nubia motion are consistent with recording the motion of a rigid or nearly rigid Danakil microplate. From these 19 spreading rates, two out of three components of the angular velocity of Arabia relative to Danakil are usefully constrained, whereas the third component, corresponding to the ridge-parallel component of surface velocity, is practically unconstrained. In this case, the use of SVD provided a way to determine which components of the angular velocity are usefully constrained and which are not.

(9) To shrink the uncertainties of the angular velocity of Arabia relative to Danakil, the slip vector from a strike-slip earthquake was incorporated, which gives a more compact confidence region that lies between poles of rotation and angular velocities previously proposed by Le Pichon & Francheteau (1978) and Sichler (1980) (but excludes both at the 95 per cent confidence level). Even with the slip vector, however, the direction of relative motion is not well constrained, the 1σ uncertainty being ± 27° at 17.0°N, 40.7°E.

(10) The angular velocity of Arabia relative to Nubia is now determined accurately enough to justify a new e ort to estimate the motion of Nubia relative to Somalia.

REFERENCES

Ambraseys, N.N., Melville, C.P. & Adams, R.D., 1994. *The Seismicity of Egypt, Arabia and the Red Sea,* Cambridge University Press, Cambridge.

Bäcker, H., Lange, K. & Richter, H., 1975. Morphology of the Red Sea Central Graben between Subair Islands and Abul Kizaan, *Geol. Jahrb. D,* **13,** 79–123.

Bosworth, W. & Taviani, M., 1996. Late Quaternary reorientation of stress field and extension direction in the southern Gulf of Suez, Egypt: evidence from uplifted coral terraces, mesoscopic fault arrays, and borehole breakouts, *Tectonics,* **15,** 791–802.

Cande, S.C. & Kent, D.V., 1992. A new geomagnetic polarity time scale for the Late Cretaceous and Cenozoic, *J. geophys. Res.,* **97,** 13 917–13 951.

Chang, T., Stock, J. & Molnar, P., 1990. The rotation group in plate tectonics and the representation of uncertainties in plate reconstructions, *Geophys. J. Int.,* **101,** 649–661.

Chase, C.G., 1978. Plate kinematics: the Americas, East Africa, and the rest of the world, *Earth planet. Sci. Lett.,* **37,** 355–368.

Cochran, J.R., 1983. A model for the development of the Red Sea, *Am. Assoc. Petrol. Geol. Bull.,* **67,** 41–69.

Coutelle, A., Pautot, G. & Guennoc, P., 1991. The structural setting of the Red Sea axial valley and deeps: implications for crustal thinning processes, *Tectonophysics,* **198,** 395–409.

DeMets, C., Gordon, R.G. & Vogt, P., 1994b. Location of the Africa–Australia–India triple junction and motion between the Australian and Indian plates: results from an aeromagnetic investigation of the Central Indian and Carlsberg ridges, *Geophys. J. Int.,* **119,** 893–930.

DeMets, C., Gordon, R.G., Argus, D.F. & Stein, S., 1990. Current plate motions, *Geophys. J. Int.,* **101,** 425–478.

DeMets, C., Gordon, R.G., Argus, D.F. & Stein, S., 1994a. E ect of recent revisions to the geomagnetic reversal time scale on estimates of current plate motion, *Geophys. Res. Lett.,* **21,** 2191–2194.

Garfunkel, Z., Ginzburg, A. & Searle, R.C., 1987. Fault pattern and mechanism of crustal spreading along the axis of the Red Sea from side scan sonar (GLORIA) data, *Ann. Geophys.,* **5B,** 187–200.

Girdler, R.W. & Southren, T.C., 1987. Structure and evolution of the northern Red Sea, *Nature,* **330,** 716–721.

Gordon, R.G., Stein, S., DeMets, C. & Argus, D.F., 1987. Statistical tests for closure of plate motion circuits, *Geophys. Res. Lett.,* **14,** 587–590.

Guennoc, P., Pautot, G. & Coutelle, A., 1988. Surficial structures of the northern Red Sea axial valley from 23°N to 28°N: time and space evolution of neo-oceanic structures, *Tectonophysics,* **153,** 1–23.

Harland, W.B., Cox, A.V., Llewellyn, P.G., Pickton, C.A.G., Smith, A.G. & Walters, R., 1982. *A Geologic Time Scale,* Cambridge University Press, New York.

Hilgen, F.J., 1991a. Extension of the astronomically calibrated (polarity) time scale to the Miocene/Pliocene boundary, *Earth planet. Sci. Lett.,* **107,** 349–368.

Hilgen, F.J., 1991b. Astronomical calibration of Gauss to Matuyama sapropels in the Mediterranean and implications for the geomagnetic polarity time scale, *Earth planet. Sci. Lett.,* **104,** 226–244.

Huang, P.Y. & Solomon, S.C., 1987. Centroid depths and mechanisms of ridge-axis earthquakes in the Indian Ocean, Gulf of Aden, and Red Sea, *J. geophys. Res.,* **92,** 1361–1382.

Izzeldin, A.Y., 1982. On the Structure and Evolution of the Red Sea, *PhD Dissertation,* Université Louis Pasteur de Strasbourg.

Izzeldin, A.Y., 1987. Seismic, gravity and magnetic surveys in the central part of the Red Sea: their interpretation and implication for the structure and evolution of the Red Sea, *Tectonophysics,* **143,** 269–306.

Izzeldin, A.Y., 1989. Transverse structures in the central part of the Red Sea and implications for the early stages of oceanic accretion, *Geophys. J.,* **96,** 117–129.

Jestin, F., Huchon, P. & Gaulier, J.M., 1994. The Somalia plate and the East African Rift System: present-day kinematics, *Geophys. J. Int.,* **116,** 637–654.

Jo e, S. & Garfunkel, Z., 1987. Plate kinematics of the circum Red Sea—a re-evaluation, *Tectonophysics,* **141,** 5–22.

LaBrecque, J.L. & Zitellini, N., 1985. Continuous sea-floor spreading in the Red Sea: an alternative interpretation of magnetic anomaly patterns, *Am. Assoc. Petrol. Geol. Bull.,* **69,** 513–524.

Le Pichon, X. & Francheteau, J., 1978. A plate tectonic analysis of the Red Sea Gulf of Aden area, *Tectonophysics,* **46,** 369–406.

Le Pichon, X. & Gaulier, J.M., 1988. The rotation of Arabia and the Levant fault system, *Tectonophysics,* **153,** 271–294.

Minster, J.B. & Jordan, T.H., 1978. Present-day plate motions, *J. geophys. Res.,* **83,** 5331–5354.

Minster, J.B., Jordan, T.H., Molnar, P. & Haines, E., 1974. Numerical modeling of instantaneous plate tectonics, *Geophys. J. R. astr. Soc.,* **36,** 541–576.

Roeser, H.A., 1975. A detailed magnetic survey of the southern Red Sea, *Geol. Jahrb.,* **D13,** 131–153.

Sandwell, D.T. & Smith, W.H.F., 1997. Marine gravity from Geosat and ERS-1 satellite altimetry, *J. geophys. Res.,* **102,** 10 039–10 054.

Schouten, H. & McCamy, K., 1972. Filtering marine magnetic anomalies, *J. geophys. Res.,* **77,** 7089–7099.

Searle, R.C. & Laughton, A.S., 1977. Sonar studies of the Mid-Atlantic Ridge and Kurchatov Fracture Zone, *J. geophys. Res.,* **82,** 5313–5328.

Sichler, B., 1980. La biellete danakile: un modèle pour l'evolution géodynamique de l'Afar, *Bull. Soc. Géol. France,* **22,** 925–933.

Simkin, T., Tilling, R.I., Taggart, J.N., Jones, W.J. & Spall, H., 1989. *This Dynamic Planet: Map of Volcanoes, Earthquakes, and Plate Tectonics,* US Geological Survey.

Simpson, R.W., 1980. A linear formulation of the plate motion problem, *Geophys. Res. Lett.,* **7,** 164–166.

Talwani, M., Windisch, C.C. & Langseth, M.G., 1971. Reykjanes ridge crest: a detailed geophysical study, *J. geophys. Res.,* **76,** 473–517.